Electronic Supplementary Material (ESI) for Physical Chemistry Chemical Physics.

Supporting Information

Signatures of Pancake Bonding in Hydrated Eumelanin

P.A. Abramov[a], O.I. Ivankov[b], A.B. Mostert[c], K.A. Motovilov[a]*

[a] Center for Photonics and 2D Materials, Moscow Institute of Physics and Technology, Institutsky Lane 9, Dolgoprudny, 141701, Moscow Region, Russia

[b] Frank Laboratory of Neutron Physics, Joint Institute for Nuclear Research, 141980 Dubna, Russia

[c] Department of Physics, Swansea University, Singleton Park, SA2 8PP, Wales, UK.

Email: *k.a.motovilov@gmail.com*

Table of Contents

1. Materials, Chemicals and Synthesis

Natural melanin from Sepia officinalis was purchased from Santa Cruz (Santa Cruz Biotechnology, Dallas, TX, USA) and used as is.

Eumelanin synthesis

Eumelanin was synthesised following a standard literature procedure [1] utilising as the initial starting material D,L-dopa (Sigma-Aldrich), which was dissolved in deionized water and subsequently adjusted to pH 8 using NH_3 (28%). Air was bubbled through the solution while being stirred for 3 d. During the synthesis, the pH would decrease due to the evaporation of NH_3, which necessitated the addition of ammonia periodically to adjust the pH back to 8. By keeping the pH ≤ 8 ensured that ring fission of the indolequinone moieties were kept to a minimum. Thus, the synthesised eumelanin can be considered a biomimetic material [2]. The solution was then brought to pH 2 using HCl (32%) to precipitate the product, which was then filtered and washed multiple times with deionized water and dried.

Cu-containing eumelanin synthesis

The synthesis of Cu-containing eumelanin was described earlier [3]. Briefly, Cu-eumelanin powder was made from the neat eumelanin powder via suspension in an aqueous Cu^{2+} solution $CuCl_2 \cdot 2H_2O$ (Sigma-Aldrich) with a target concentration of 1 Cu^{2+} mmol per gram of eumelanin. The suspension time was for 3 days. The suspension was filtered, washed with deionised water and dried.

X-ray Photoemission Spectroscopy (XPS)

XPS was obtained via a wide-scan survey spectrum of pressed pellets of the powder utilising a Kratos Axis Supra (Shimadzu, Japan) with a 225 W AlKα X-ray source with an emission current of 15 mA and equipped with a quartz crystal monochromator with a 500 mm Rowland circle. Higher resolution spectra were then collected in triplicate with a pass energy of 40 eV, with the hybrid lens setting, 0.1 eV step size, 1 s dwell time for electron counting at each step. The integral Kratos charge neutralizer was used as an electron source to eliminate differential charging. Atomic compositions can be seen in **Supplementary Table S1**. The values are compatible with that of a synthetic eumelanin, with 70% DHI/ 30% DHICA content. We note that elemental surface scans of eumelanins are representative of the bulk as previously demonstrated, with the exception of Cu content, which can't be quantified readily within eumelanin samples [4]. The high-resolution scans are given in Supplementary **Fig. S1 & Fig. S2**. The fitting followed previous work [4] and would indicate a material that is more quinone heavy, i.e. highly oxidised, as would be expected for the synthesis conditions. Furthermore, the low intensity from peaks associated with carboxyl groups is consistent with the elemental analysis.

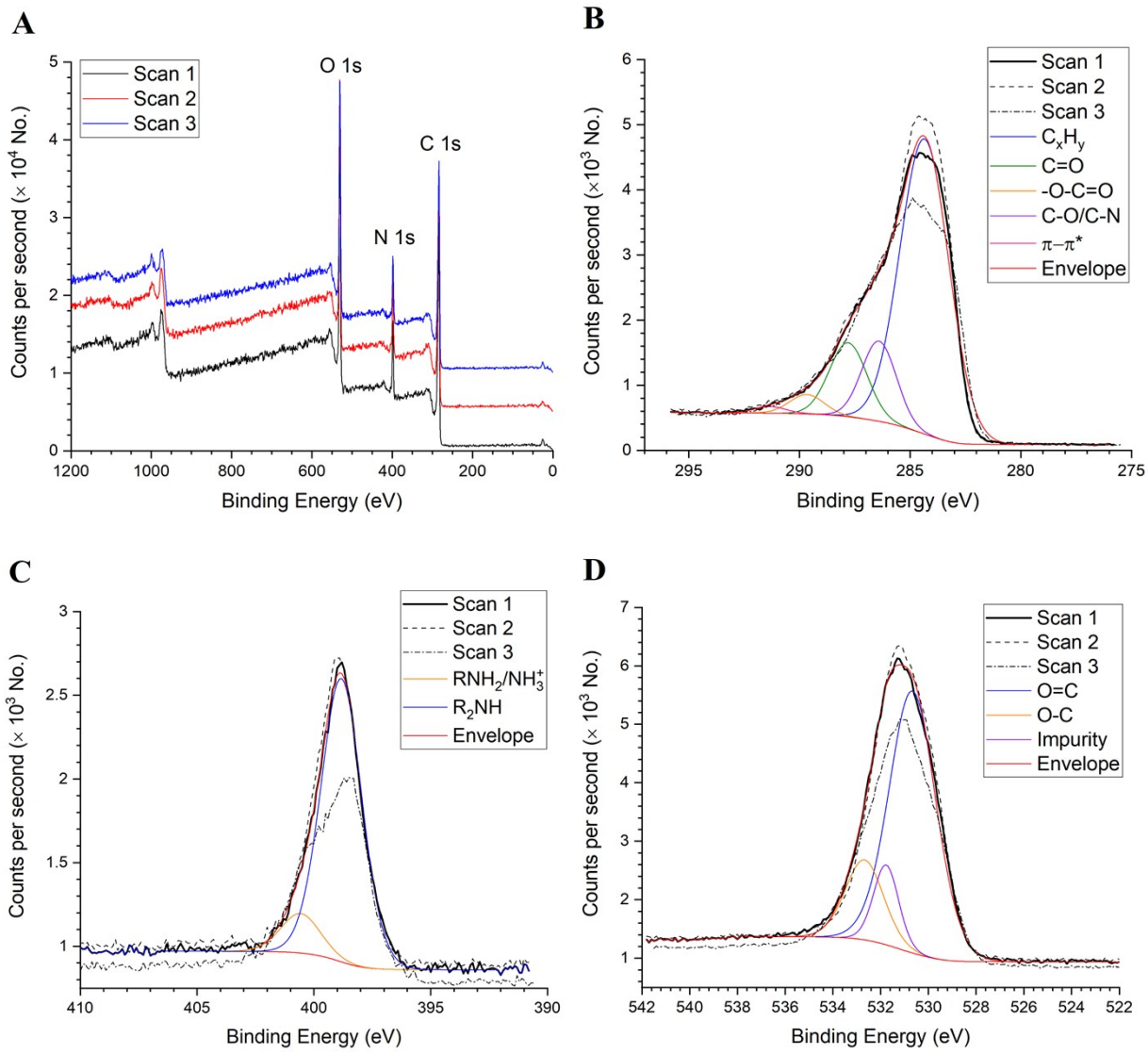

Supplementary Fig. S1 - XPS scans of the neat, synthetic eumelanin. Three scans were performed and binding energies were calibrated such that the peak of the C 1s was fixed to 284.4 eV. A) Wide survey scans show peaks at C 1s, N 1s and O 1s. B) The high resolution C 1s peak. The three data sets are shown, and modelling done on scan data set 1 (bolded) shows 5 contributing peaks. Peak assignment follows [4]. As can be seen, there is some contribution from -O-C=O, indicating DHICA moieties are present, consistent with the broad elemental analysis in Table S1. C) The high resolution N 1s peak, with modelling on one of the 3 data sets. D) The high resolution O 1s peak, with modelling on one of the 3 data sets. The domination of O=C over O-C would tend to indicate an abundance of quinone units vis-à-vis hydroquinone/catechol units.

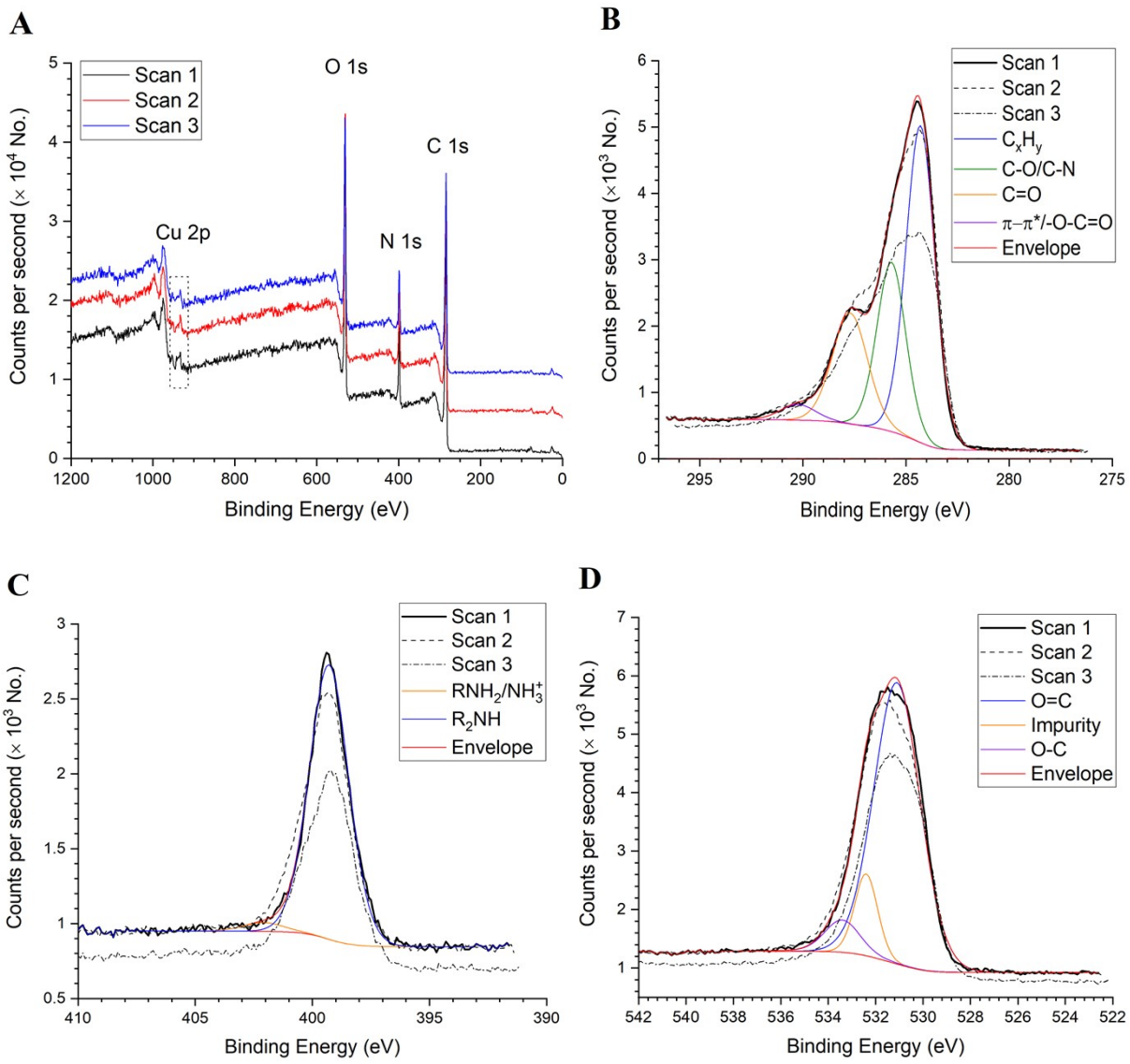

Supplementary Fig. S2 - XPS scans of the Cu chelated synthetic eumelanin. Three scans were performed and binding energies were calibrated such that the peak of the C 1s was fixed to 284.4 eV. A) Wide survey scans show peaks at C 1s, N 1s and O 1s as well as the presence of the Cu 2p peak as would be expected. B) The high resolution C 1s peak. The three data sets are shown, and modelling done on scan data set 1 (bolded) shows contributing peaks unlike the neat material, since the π-π* shake-up peak can't be distinguished from the -O-C=O peak. Peak assignment follows [4]. C) The high resolution N 1s peak, with modelling on one of the 3 data sets. D) The high resolution O 1s peak, with modelling on one of the 3 data sets. The domination of O=C over O-C would tend to indicate an abundance of quinone units vis-à-vis hydroquinone/catechol units. No elemental analysis was done on the Cu peak, since the Cu^{1+} and Cu^{2+} can't be accurately quantified [3,4].

Supplementary Table S1 - Elemental analysis results from the XPS scans. Shown are the theoretical values one would expect if one had either a pure poly DHI or poly DHICA. Data indicates a material that is 70% DHI and 30% DHICA, in line with a synthetic eumelanin, though a bit DHICA rich since most synthetics contain ~ 10% DHICA [2].

	Mean (%)	StDev (%)	DHI / DHICA fraction
Theoretical DHI			1.0 / 0
Carbon	72.7	-	
Nitrogen	9.1	-	
Oxygen	18.2	-	
Theoretical DHICA			0 / 1.0
Carbon	64.3	-	
Nitrogen	7.1	-	
Oxygen	29.6	-	
Neat Eumelanin			0.7 / 0.3
Carbon	69.6	0.4	
Nitrogen	9.1	0.1	
Oxygen	21.3	0.3	
Cu Eumelanin			0.7 / 0.3
Carbon	69.6	0.5	
Nitrogen	9.4	0.2	
Oxygen	20.9	0.4	

Elemental analysis performed by inductively coupled plasma atomic emission spectroscopy (ICP-AES) and inductively coupled plasma mass spectrometry (CP-MS).

To obtain elemental values for the metal ion content in the studied synthetic eumelanins specifically, we used ICP-AES and CP-MS. An iCAP-6500 Duo (Thermo Scientific, USA) spectrometer was used for the atomic-emission determination of elements at the following working parameters: plasma power 1250 W, a VeeSpray nebulizer, a spray chamber of cyclone type, a plasma Ar flow of 12 l/min and an auxiliary Ar flow of 0.5 l/min, a nebulizer Ar flow of 0.5 l/min, the analysed sample flow of 1.8 ml/min. Mass-spectral determination of elements was made with a XSeries 2 quadrupole mass-spectrometer (Thermo Scientific, USA) at the following working parameters: plasma power of 1300 W, a set of standard nickel cones, a Polycon concentric sprayer, a quartz spraying chamber cooled to 3°C, the plasma Ar flow of 13 l/min, and an auxiliary Ar flow of 0.9 l/min, the nebulizer Ar flow of 0.95 l/min and the the analysed sample flow of 0.8 ml/min.

Samples were prepared via digestion. The following acids were used to dissolve samples: HNO_3 (nitric acid 65 %; max. 0,0000005 % Hg; GR, ISO), HCl (hydrochloric acid 37%; max. 0,0000005 % Hg; PA-ACS-ISO; Panreac, Spain). Also utilised was deionised water (18.2 MΩ) and solutions of multielement and single-element standards of High-Purity Standards, USA. The solutions were stored in 15 ml polyethylene tubes (Labcon, USA). All the tubes were first kept in 5% HNO_3 for 4-5 days and washed with deionised water directly before using. The samples were dissolved in an autoclave system (IMT RUS, Russia). These autoclave systems enable heating 30 cm^3 teflon reaction chambers to the maximum temperature of 240°C and pressure of 20 MP (200 bars).

Sample digestion was performed using batches of 6 samples with the mass of each ranging from 20 to 50 mg. Each batch contained one control sample in addition to the analysed one. Samples were placed into the Teflon reaction chambers in the autoclave and 1 ml of HNO_3 and 0.2 ml of HCl were added to the chambers. The chambers were closed with caps and evacuated in the autoclave titanium housings. The autoclaves were placed in an electric furnace and held at 160°C (1h), 180°C (1h), 200°C (1h). After cooling the autoclaves were opened, the solutions were then transferred to polyethylene test tubes and then each solution volume was brought up to 10 ml using deionised water. The solutions from the reaction chambers without an analysed sample were used as a control. Before measurements all the solutions were diluted by 2-5 times and an internal standard of 10 μg/l In was added.

The full list of determined elements and their concentrations is given in **Supplementary Table S2**.

Supplementary Table S2. Elemental analysis results for the Cu-containing synthetic eumelanin obtained by inductively coupled plasma atomic emission spectroscopy (ICP-AES) and inductively coupled plasma mass spectrometry (CP-MS).

Element	**Detection limit, µg/g**	**Concentration, µg/g**	
		Neat eumelanin	**Cu-doped eumelanin**
Li	0.01	0.021	< DL
Be	0.003	< DL	< DL
B	0.6	26.3	6.5
Na	4	16.2	5.6
Mg	3	< DL	< DL
Al	4	20.6	24.8
P	10	< DL	< DL
S	29	145	< DL
K	3	4.5	6.5
Ca	22	< DL	< DL
Sc	0.1	< DL	< DL
Ti	2	< DL	< DL
V	1	< DL	< DL

Cr	0.5	12.9	2.7
Mn	0.2	3.3	2.2
Fe	5	49.5	197
Co	0.1	< DL	< DL
Ni	0.2	0.89	0.86
Cu	0.3	15.3	40491
Zn	0.2	7.1	1.7
Ga	0.05	< DL	< DL
Ge	0.1	< DL	< DL
As	0.03	< DL	< DL
Se	0.8	< DL	< DL
Rb	0.05	< DL	< DL
Sr	0.04	0.10	0.12
Y	0.06	< DL	< DL
Zr	0.03	1.1	1.6
Nb	0.08	< DL	< DL
Mo	0.01	0.38	0.78

Rh	0.07	< DL	< 0.7
Pd	0.08	< DL	< DL
Ag*	0.1	124	< DL
Cd	0.02	< DL	< DL
Sn	0.05	0.89	12.0
Sb	0.02	0.056	0.12
Te	0.02	< DL	< DL
Cs	0.004	< DL	< DL
Ba	0.01	1.3	28.5
La	0.002	0.0088	0.041
Ce	0.003	0.020	0.032
Pr	0.002	< DL	0.0020
Nd	0.002	0.010	0.0064
Sm	0.002	0.0073	< DL
Eu	0.003	< DL	0.0044
Gd	0.001	< DL	< DL
Tb	0.002	< DL	< DL

Dy	0.002	< DL	< DL
Ho	0.001	< DL	< DL
Er	0.001	< DL	< DL
Tm	0.001	< DL	< DL
Yb	0.002	< DL	< DL
Lu	0.001	< DL	< DL
Hf	0.01	0.022	0.036
Ta	0.004	< DL	< DL
W	0.02	0.19	0.49
Re	0.002	< DL	< DL
Ir	0.002	< DL	< DL
Pt	0.003	< DL	0.010
Au	0.01	0.031	< DL
Hg	0.02	0.18	< DL
Tl	0.003	< DL	< DL
Pb	0.03	0.30	2.6
Bi	0.004	0.028	0.032

Th	0.004	< DL	< DL
U	0.001	0.0044	0.0057

2. X-Ray Diffraction Measurements Using 2Θ Scheme

X-ray powder diffraction measurements were performed on ARL X'TRA X-ray diffractometer (manufactured by Thermo Scientific, USA) with source tube using Cu-anode and K_α with λ = 1.540562 Å in 2Θ reflection configuration. To achieve and stabilise the needed hydration level of material we placed XRD drone cuvette with powder eumelanin into the camera with water vapour equilibrated over saturated solutions of LiCl, KCl salts (corresponding values of relative humidity (RH) 12% and 84% respectively) for 18-20 hours at room temperature 24 ± 2 °C and in the ambient environment. Then we move the cuvette in a sealed container to the diffractometer. Right before the diffraction measurement, we removed a lid from the sample container. The prepared samples were examined in a 2θ scanning regime in a range of 2 to 40 degrees (44.16 Å and 2.25 Å respectively). Provided data on the **fig. S3** corresponds to a signal accumulation time of 1 second with an angle step Δ = 0.05°. The full measurement process took less than 10 minutes per measurement. We assume that during this time, changes in the water content of the material were insignificant. The diffractogram of the empty cell was collected as a background and subtracted afterward. For the peak finding we subtract the background, and afterward, smooth the data with a Savitzky–Golay filter (window size = 10). Then with the automatic SciPy peak finder function we get the local maximum.

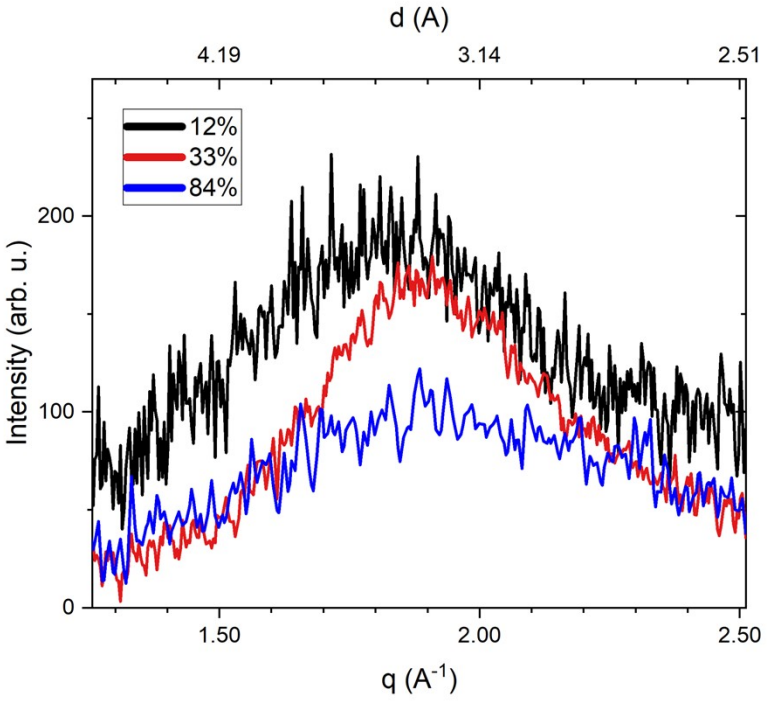

Supplementary Fig. S3. Wide-angle x-ray powder diffraction data obtained in 2**θ** configuration for the neat synthetic eumelanin at different relative humidity level conditions (12%, 33% and 84%).

3. X-Ray Diffraction Measurements Using Absorption Scheme

The WAXS measurements were carried out using the Xeuss 3.0 SAXS/WAXS System (manufactured by Xenocs SAS, France) operating in point geometry equipped with a GeniX^{3D} microfocus generator of X-ray radiation with source Mo-Kα (λ = 0.71078 Å). **Fig. S4** represents photos of the general system view and capillary sample holder. The spectrometer was equipped with a moving detector Eiger2 R 1M 2D-detector (Dectris) with a sensitive area of 77.1 × 79.7 mm^2 and integrated with the XSACT program. The measurements using 46 mm sample-to-detector distance allows one to obtain the X-ray scattering intensity I(q) in the range of momentum transfer of approximately ~1< q < ~8 Å^{-1}. The measurements were carried out in vacuum at room temperature in the borosilicate glass capillaries (Hilgenberg, Germany, 0.1 mm wall thickness, 1.5 mm flight path). To keep particular material under the stable hydration level conditions we placed it in a capillary. Then, the capillary was kept in vacuum or in the water vapour equilibrated over saturated solutions of $Na_2Cr_2O_7$, KCl, pure H_2O (corresponding values of relative humidity 54 and 84% respectively) for 18-20 hours. Afterwards, capillaries were flame sealing.

Supplementary Fig. S4. Photos of the Xeuss 3.0 SAXS/WAXS System (installed and operated in FLNP, JINR, Dubna) used for acquiring the main XRD data. On the left side is the general view of the system and on the right is the sample holder with capillaries containing hydrated eumelanins.

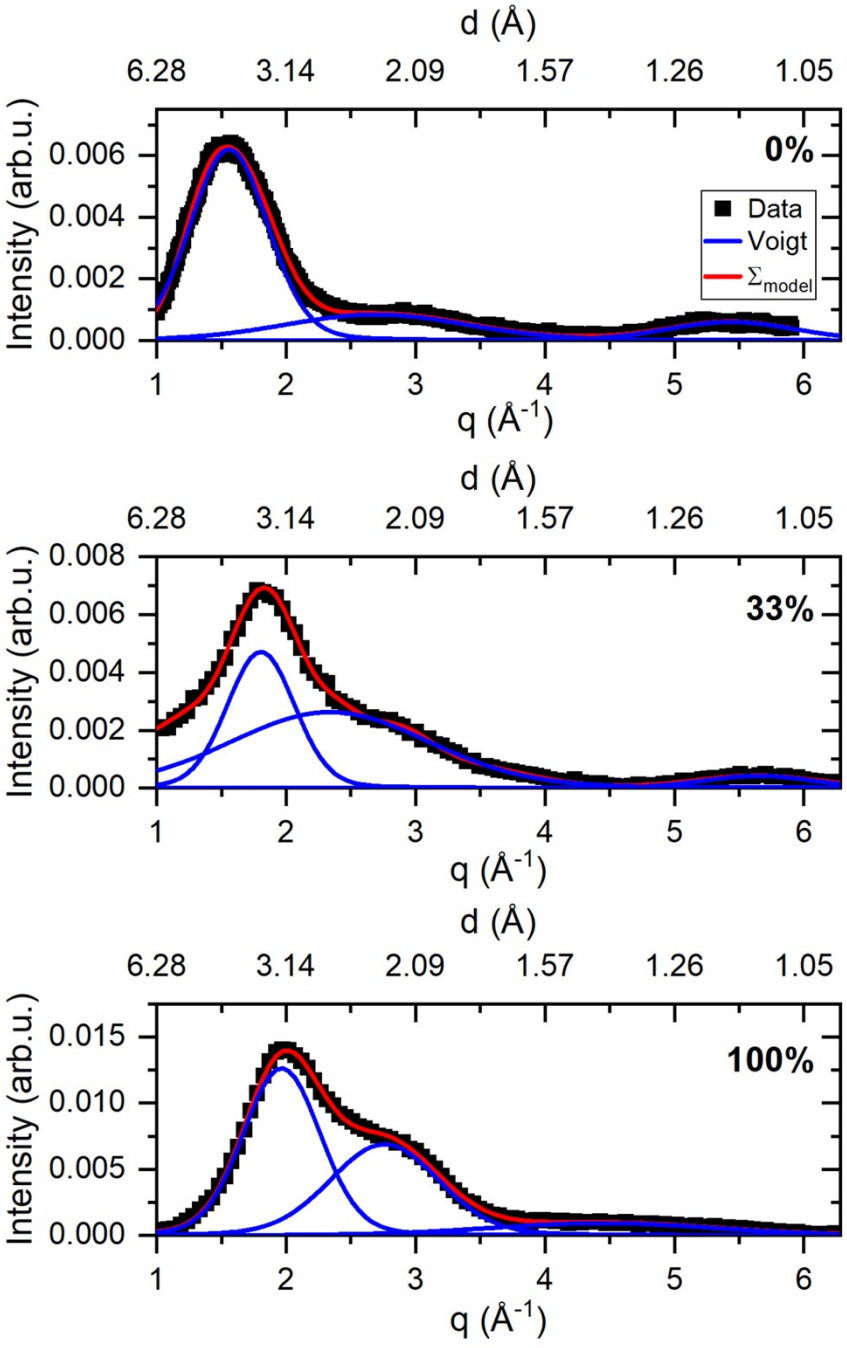

Supplementary Fig. S5. Wide-angle x-ray diffraction data for the neat synthetic eumelanin at different relative humidity level conditions (vacuum, 33% and 100%). The exact value of relative humidity utilised for the sample preparation is given in the upper right corner of each graph. Black squares correspond to raw data, blue lines are results of modelling data with Voigt profiles, red lines are sums of corresponding Voigt profiles.

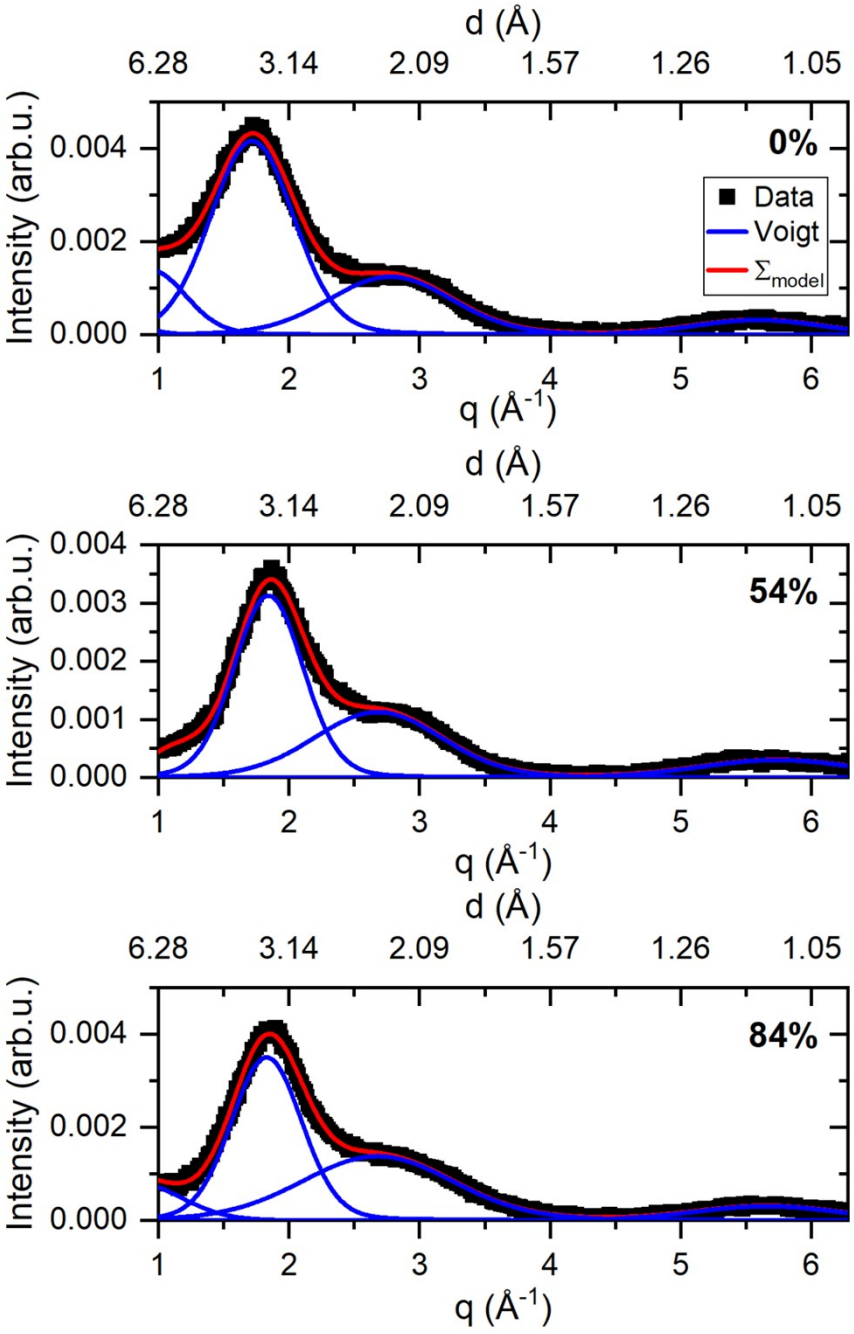

Supplementary Fig. S6. Wide-angle x-ray diffraction data for the Cu-containing synthetic eumelanin at different relative humidity level conditions (vacuum, 54% and 84%). The exact value of relative humidity utilised for the sample preparation is given in the upper right corner of each graph. Black squares correspond to raw data, blue lines are results of modelling data with Voigt profiles, red lines are sums of corresponding Voigt profiles.

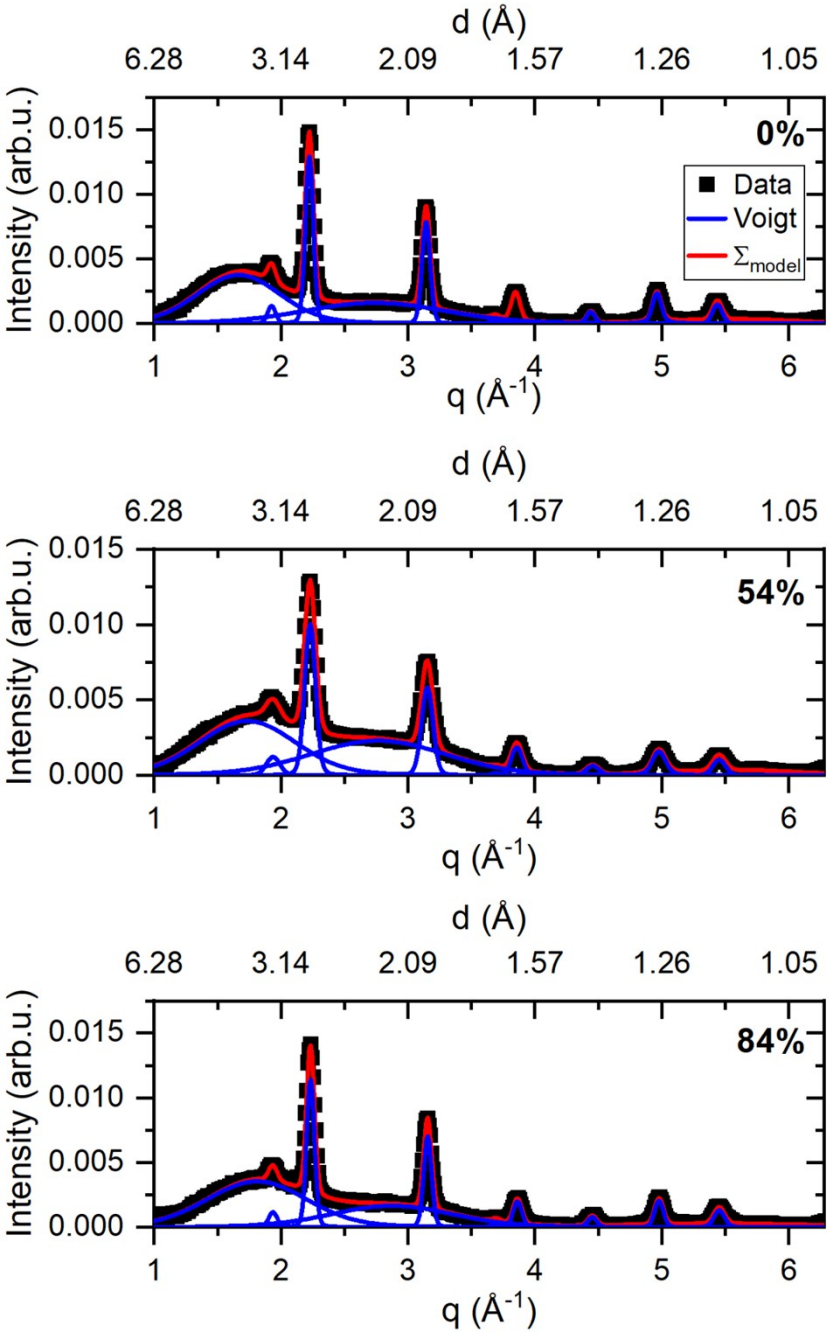

Supplementary Fig. S7. Wide-angle x-ray diffraction data for the natural eumelanin from *Sepia officinalis* at different relative humidity level conditions (vacuum, 54% and 84%). The exact value of relative humidity utilised for the sample preparation is given in the upper right corner of each graph. Black squares correspond to raw data, blue lines are results of modelling data with Voigt profiles, red lines are sums of corresponding Voigt profiles.

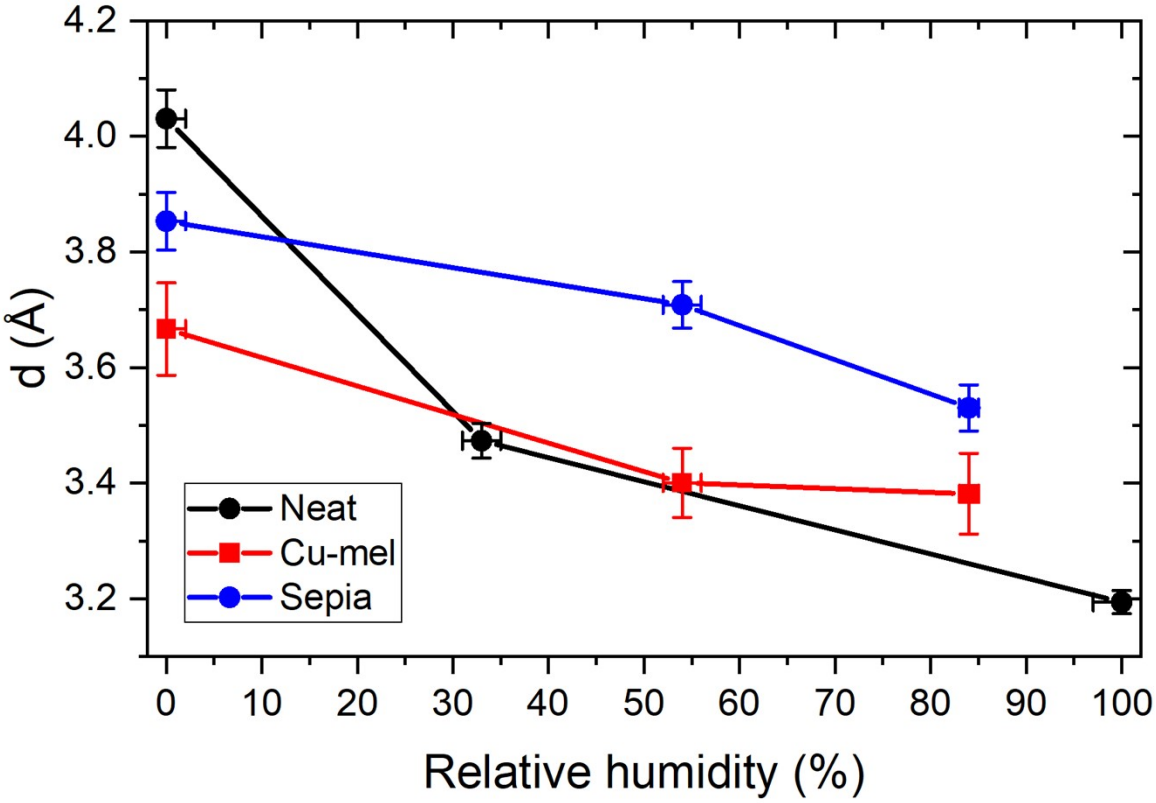

Supplementary Fig. S8. Positions of the scattering peak centre responsible for the mean d_{π} value obtained from wide-angle x-ray diffraction data for the studied eumelanins with respect to the level of relative humidity (RH). The black curve corresponds to values obtained for the neat synthetic eumelanin (fig. S5), the red curve represents the Cu-containing synthetic eumelanin, and the blue curve is responsible for the *Sepia officinalis* natural eumelanin.

Supplementary Table S3. The π-stack peak positions, i.e. values of mean d_π, for studied eumelanins depending on the relative humidity (RH).

RH, %	Neat-Mel	Cu-Mel	*S.officinalis*
0	4.031	3.656	3.770
33	3.478	--	--
54	--	3.434	3.623
84	--	3.408	3.472
100	3.194	--	–
Δ	**0.837**	**0.248**	**0.298**

Supplementary Table S4. The evolution of narrow peaks positions for *Sepia officinalis* eumelanin depending on the value of relative humidity (RH).

Peak #	0%-RH	54%-RH	84%-RH
1	3.26	3.24	3.24
2	2.83	2.82	2.81
3	2.00	1.99	1.99
4	1.70	1.70	1.70
5	1.63	1.63	1.63
6	1.41	1.41	1.41
7	1.27	1.26	1.26
8	1.16	1.15	1.15
9	1.13	1.12	1.15

4. The Measurements of Eumelanin Swelling Induced by Hydration

To prepare eumelanin films we dissolved eumelanin powder in an ammonia-water solution with a volume ratio of 1 (eumelanin) : 14 (NH_3): 7 (H_2O) and ultrasonicated it as described elsewhere [5]. We deposited the solution on an optically polished CaF_2 substrate by spraying. The resulting film was crumble and heterogeneous in thickness (from 1.5 microns to 2.5 microns). The flakes had a profile concave to the centre (**Fig. S9**).

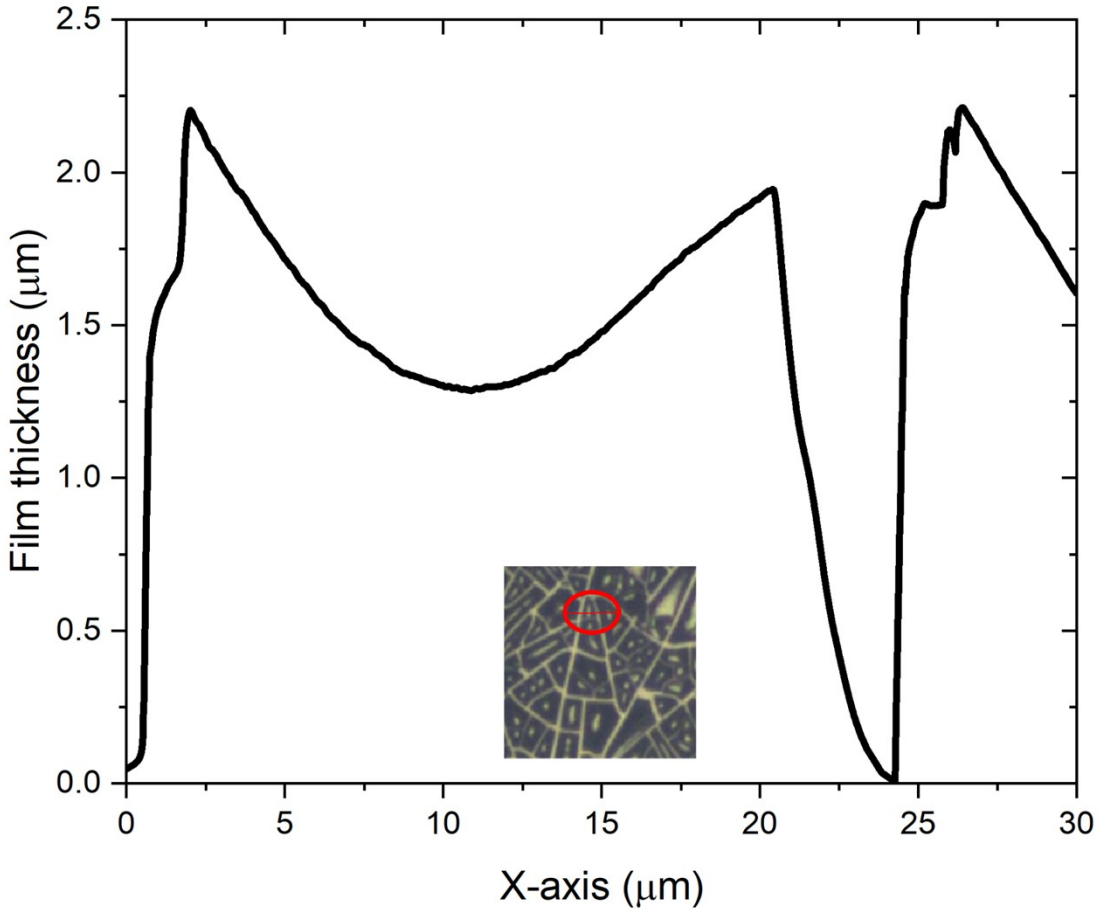

Supplementary Fig. S9. The height profile of one of the eumelanin film's flakes obtained by atomic-force microscopy. The studied flake is shown in the inset.

We placed the sample in a specially manufactured sealed chamber with CaF_2 optical windows described earlier [6]. The chamber has inlet and outlet hoses for the wet air supply provided via a membrane pump. To stabilise the hydration level we utilised saturated aqueous solutions of LiCl, $MgCl_2$, $Na_2Cr_2O_7$, NaCl, KCl at temperature 24 ± 1 °C. The corresponding values of relative humidity above the listed systems were 13, 33, 54, 75, and 84% RH respectively. The values of relative humidity (RH) and temperature were monitored during the experiment with the Si7021 sensor (Adafruit, USA). The changes of eumelanin films' area induced by the alternation of humidity level were observed in an optical microscope equipped with a digital camera (DS-Fi2 Nikon, Japan). An optically transparent substrate can be observed through the cracks. Example photos of the film are presented on **fig. S10**. Using the algorithmic estimation of the ratio of the areas of the transparent substrate and the opaque eumelanin film, one can judge the degree of film swelling. To calculate the corresponding areas we processed the obtained images with the OpenCV python module[7].

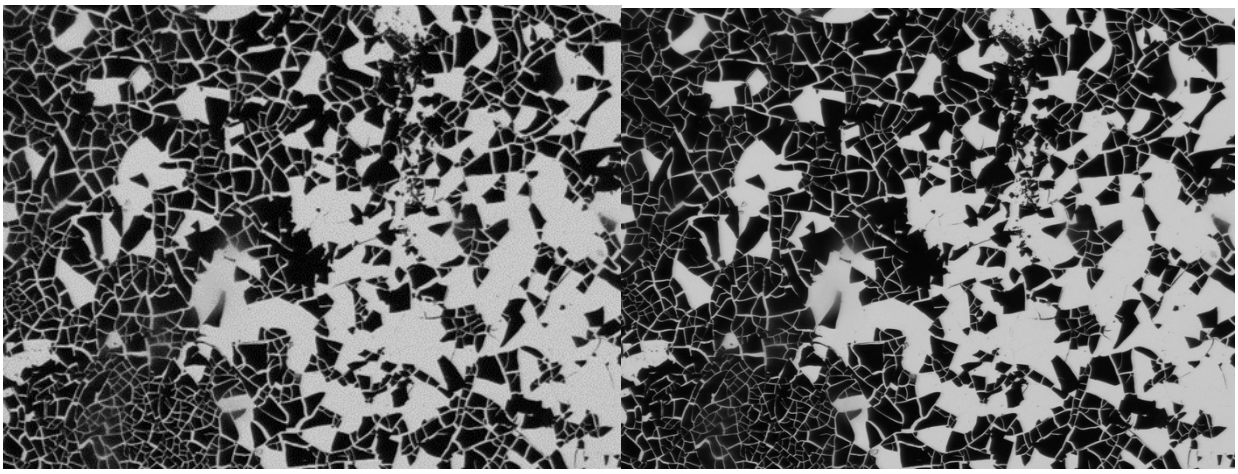

Supplementary Fig. S10. Example photos of the thick neat synthetic eumelanin film at 13% (left) and 84% (right) relative humidity at 22 ^{o}C used to estimate the hydration-induced growth.

5. Hydration-induced changes of eumelanin parameters and their correlations

In the framework of the current ESI chapter we want to make additional clarification of the data presented on fig.4 of the main text. We performed the conversion from units of relative air humidity (RH), used in the current study, to absolute values of water concentration in eumelanin using the data from the article[7] in which the absorption curve was obtained for eumelanin pressed powder pellets. It also should be taken into account that water sorption by 30 nm films[8] and by powders[9] have similar profiles. We emphasise that muon spin relaxation (muSR)[10], electron paramagnetic resonance (EPR)[11] and current PB phenomenology studies were performed on powder or pressed powder eumelanin.

The eumelanin swelling process was examined on a thick film (see the SI chapter 4). We assume that for thick films, which are an intermediate state between thin films and pressed powder, the same absorption data can be used.

Normalised free-radical spin concentration for fig. 4A in the current study's main text was extracted directly from figure 2D in the referenced article[11]. It corresponds to neat synthetic eumelanin hydrated at neutral pH. The concerned reader may see that the radical density R_D and interlayer distance d_π in π-stacks in eumelanin decrease in a very similar manner (fig. 4A, main text).

The hydration-dependent values of paramagnetic muSR component λ for fig. 4B of the current study's main text were extracted directly from fig. 1B of the referenced article[10]. The deeper analysis and description of muSR-based methods' capabilities and limitations can be found in the recently published book[12]. Since in the neat synthetic eumelanin additional paramagnetic centres like paramagnetic metal cations are absent, we regard the behaviour of λ as a characteristic of the concentration of the intrinsic radicals in the material. The fundamentally different results of the EPR spin concentration and muSR λ parameter with respect to the increase in humidity is an old contradiction in the results obtained on eumelanin. We think that PB phenomenology allows this contradiction to be resolved as explained in the main text.

Finally, highlighting the hydration-induced swelling of the eumelanin film as demonstrated in fig. 4C, leads us to speculate that there may be at least two levels of structural organisation in eumelanin. The observed paradox between the different hydration response behaviours of the total volume and the interplanar stack distance can only be resolved by taking into account two levels of structure. At the level of nanoscale clusters, the distances between the layers of π-systems are compressed. At the larger scale the increase in volume is due to the absorption of water between the particles. In this sense, it is incorrect to speak of water-induced destacking in eumelanin. It is more accurate to speak of water-induced loosening at the mesoscopic level of the structure.

6. References

1 C. C. Felix, J. S. Hyde, T. Sarna and R. C. Sealy, Interactions of melanin with metal ions. Electron spin resonance evidence for chelate complexes of metal ions with free radicals, *J. Am. Chem. Soc.*, 1978, **100**, 3922–3926.

2 M. d'Ischia, K. Wakamatsu, A. Napolitano, S. Briganti, J.-C. Garcia-Borron, D. Kovacs, P. Meredith, A. Pezzella, M. Picardo, T. Sarna, J. D. Simon and S. Ito, Melanins and melanogenesis: methods, standards, protocols, *Pigment Cell & Melanoma Research*, 2013, **26**, 616–633.

3 A. B. Mostert, S. B. Rienecker, M. Sheliakina, P. Zierep, G. R. Hanson, J. R. Harmer, G. Schenk and P. Meredith, Engineering proton conductivity in melanin using metal doping, *J. Mater. Chem. B*, , DOI:10.1039/D0TB01390K.

4 J. V. Paulin, J. D. McGettrick, C. F. O. Graeff and A. B. Mostert, Melanin system composition analyzed by XPS depth profiling, *Surfaces and Interfaces*, 2021, **24**, 101053.

5 J. P. Bothma, J. de Boor, U. Divakar, P. E. Schwenn and P. Meredith, Device-Quality Electrically Conducting Melanin Thin Films, *Advanced Materials*, 2008, **20**, 3539–3542.

6 Z. V. Bedran, S. S. Zhukov, P. A. Abramov, I. O. Tyurenkov, B. P. Gorshunov, A. B. Mostert and K. A. Motovilov, Water-Activated Semiquinone Formation and Carboxylic Acid Dissociation in Melanin Revealed by Infrared Spectroscopy, *Polymers*, 2021, **13**, 4403.

7 A. B. Mostert, K. J. P. Davy, J. L. Ruggles, B. J. Powell, I. R. Gentle and P. Meredith, Gaseous Adsorption in Melanins: Hydrophilic Biomacromolecules with High Electrical Conductivities, *Langmuir*, 2010, **26**, 412–416.

8 A. J. Clulow, A. B. Mostert, M. Sheliakina, A. Nelson, N. Booth, P. L. Burn, I. R. Gentle and P. Meredith, The structural impact of water sorption on device-quality melanin thin films, *Soft Matter*, 2017, **13**, 3954–3965.

9 J. A. Martinez-Gonzalez, H. Cavaye, J. D. McGettrick, P. Meredith, K. A. Motovilov and A. B. Mostert, Interfacial water morphology in hydrated melanin, *Soft Matter*, 2021, **17**, 7940–7952.

10 A. B. Mostert, B. J. Powell, F. L. Pratt, G. R. Hanson, T. Sarna, I. R. Gentle and P. Meredith, Role of semiconductivity and ion transport in the electrical conduction of melanin, *PNAS*, 2012, **109**, 8943–8947.

11 A. B. Mostert, G. R. Hanson, T. Sarna, I. R. Gentle, B. J. Powell and P. Meredith, Hydration-Controlled X-Band EPR Spectroscopy: A Tool for Unravelling the Complexities of the Solid-State Free Radical in Eumelanin, *J. Phys. Chem. B*, 2013, **117**, 4965–4972.

12 S. J. Blundell, R. D. Renzi, T. Lancaster and F. L. Pratt, Eds., *Muon Spectroscopy: An Introduction*, Oxford University Press, New York, 2022.